Automated Pre–processing Method for Dermoscopic Images and its Application to Pigmented Skin Lesion Segmentation

Ali Madooei, Mark S. Drew, Maryam Sadeghi, and M. Stella Atkins
School of Computing Science
Simon Fraser University
{***amadooei, mark, msa68, stella***}***@cs.sfu.ca***
http://www.cs.sfu.ca/∼amadooei

Abstract

In this paper, we put forward a new pre–processing scheme for automatic analysis of dermoscopic images. Our contributions are two-fold. First, we present a procedure, an extension of previous approaches, which succeeds in removing confounding factors from dermoscopic images: these include shading induced by imaging non-flat skin surfaces and the effect of light-intensity falloff toward the edges of the dermoscopic image. This procedure is shown to facilitate the detection and removal of artifacts such as hairs as well. Second, we present a novel simple yet effective greyscale conversion approach that is based on physics and biology of human skin. Our proposed greyscale image provides high separability between a pigmented lesion and normal skin surrounding it. Finally, using our pre–processing scheme, we perform segmentation based on simple grey-level thresholding, with results outperforming the state of the art.

1. Introduction

Melanoma in particular along with other malignant skin cancers are among the most rapidly increasing cancers in the world, with high mortality rate [1]. Early detection of melanoma is very important, particularly before the metastasis phase when the cancer is still localized and it can be completely cured with surgical excision. Unfortunately, clinical diagnosis of melanoma is difficult even for experienced dermatologists [2]. Therefore, there is an increasing demand for computer-aided diagnostic systems to catch early melanomas.

A popular imaging method for diagnosis and early screening of pigmented skin lesions is dermoscopy. Inevitably, most efforts in computerizing diagnosis of melanoma lean towards automatic analysis of dermoscopic images. The latter typically involves successive steps of: pre–processing, segmentation, feature extraction, feature selection and classification.

The pre–processing, which is the focus of this study, is an important step that tends to facilitate the segmentation process. Segmentation, i.e. isolating skin lesions from normal skin surrounding it, is a crucial step itself that will affect all downstream processes and even the final diagnosis. For example, the presence of artifacts, such as hair, in the image may disturb the identification of a lesion's morphological features. Therefore a pre–processing of artifact–removal can considerably contribute to the accuracy of each step, improving the overall performance.

In the following, we propose a new pre–processing scheme for automatic analysis of dermoscopic images. Our contributions are two-fold. First, we present a procedure, an extension of previous approaches, which succeeds in attenuation of shading induced by imaging non-flat skin surfaces and the effect of light-intensity falloff toward the edges of the dermoscopic image. We discuss how this procedure might facilitate the detection and removal of artifacts such as hairs. Next, we present a simple yet effective novel approach to convert a colour dermoscopic image (typically in sRGB) into a greyscale one. Our greyscale conversion approach is based on biological and optical properties of human skin and the physics of image formation. Finally, we demonstrate the effectiveness of our proposed pre–processing scheme by performing segmentation based on simple grey-level thresholding, with results outperforming the state of the art.

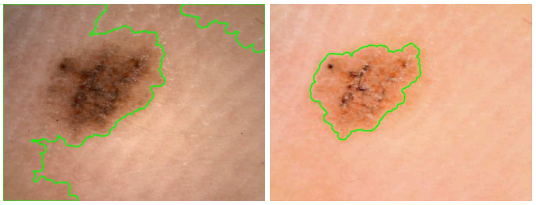

(a) (b)

Figure 1. *(a) input image (the lesion is completely in the shaded area); (b) after shading attenuation by our approach – The green border is the lesion boundary detected by Otsu's grey-level thresholding method.*

2. Attenuation of Confounding Factors

Pre–processing methods used for dermoscopy images are of many kinds, including but not limited to: colour calibration [3], colour-space transformation [4], removal of artifacts (such as hairs, ruler markings, air bubbles, black frames, ink markings, etc.) [5]. Among these, previous efforts have mostly been focused on development of hair removal algorithms (e.g. [5, 6])

Shading and light-intensity falloff toward the edges of dermoscopic image is one of the less studied confounding factors. This could cause colour degradation, and radically alter segmentation results. See Fig. 1 for an example. Shading is induced by imaging non-flat skin surfaces, and intensity falloff is due to diffraction of light such that the image is brighter near the center and darker near the edges (the illumination may deviate from the center of the image according to the angle between the dermoscope and the skin).

To our knowledge, the only study that directly addresses shading attenuation for dermoscopy images, is the one by Cavalcanti et al. [7]. Their approach is an attempt to estimate the illumination as a quadratic function of image coordinates and then spatially normalizing it. According to their own evaluation of the method, "it has limited affect on local cast shadows, fails on sur-

face shapes that are not locally smooth and works best when the illumination varies slowly across the scene" [7]. We also point out that their method is highly constrained by its assumptions and methodology: i) the method assumes the lesion is in the center of the image and the corners of the image contains only healthy skin. Further, a window of size 20×20 pixel at each corner is used to estimate the illumination function. While this seems to be working on the few sample images provided in their paper, it would incorrectly estimate the illumination function for images containing hairs or other artifacts in the corner areas (such as Fig. 2(a)). ii) their method works best when the illumination varies (smoothly) from one corner to another. However, it works poorly when the corners are relatively equally darker than the center of the image, which is the case for most dermoscopy images, especially those suffering from intensity falloff (as described earlier).

We begin by following [7] by normalizing the Value channel of HSV and then converting the image from HSV colour space to the original RGB. However, we normalize V, as will be described shortly, with respect to the *intrinsic image* [8] of the original image. In computer vision, images with lighting removed are denoted as "intrinsic". In line with [8], we use the entropy minimization technique to find the intrinsic image. Our tests demonstrate that the proposed method overcomes the limitations of [7] while succeeded in removing or strongly attenuating shading and intensity falloffs.

In the rest of this section, the theory of intrinsic images is briefly described, followed by our approach for normalizing Value channel (of HSV), and eventually attenuating shading and other confounding lighting effects.

2.1 Image Formation

In keeping with [8] we adopt a standard model in computer vision for colour image formation. Suppose the illuminant spectral power distribution is $E(\lambda)$ and, in any reflective case, the spectral reflectance function at pixel (x,y) is $S(x,y,\lambda)$. Then measured RGB values are given by

$$R_k(x,y) = \omega(x,y) \int E(x,y,\lambda_k) S(x,y,\lambda_k) Q_k(\lambda) d\lambda \qquad (1)$$

where $k = 1..3$, ω denotes shading variation (e.g., Lambertian shading is surface normal dotted into light direction, although we do not assume Lambertian surfaces here); and $Q_k(\lambda)$ is the camera sensor sensitivity functions in the R,G,B channels.

Following [8] we adopt a simple model for the illuminant: we assume the light can be written as a Planckian radiator (in Wien's approximation):

$$E(x,y,\lambda,T) \simeq I(x,y) k_1 \lambda^{-5} exp(-k_2/(T\lambda)) \qquad (2)$$

where k_1 and k_2 are constants, T is the correlated colour temperature characterizing the light spectrum, and I is the lighting intensity at pixel (x,y), allowing for a possible rolloff in intensity towards the periphery of the dermoscopic image. We assume light temperature T is constant across the image (but is, in general, unknown).

In line with [8] we assume camera sensors are narrowband or can be made narrowband via a spectral sharpening operation [9]. In this approximation, sensor curve $Q_k(\lambda)$ is simply assumed to be a delta function: $Q_k(\lambda) = q_k \delta(\lambda - \lambda_k)$, where specific wavelengths λ_k and sensor-curve heights q_k are properties of the camera used. To this end we simplify 1 by substituting $E(x,y,\lambda)$ and $Q_k(\lambda)$:

$$R_k = \sigma I k_1 \lambda^{-5} e^{-\frac{k_2}{T\lambda}} S(\lambda_k) q_k, \qquad (3)$$

The effect of shading and illumination can be eliminated from eq.(3) by dividing to get the band-ratio 2-vector chromaticities $c_k = R_k/R_p$ where p is fixed to one colour channel (usually the green channel), and k indexes over the other two channels (red and blue).

Note that the effects of the illumination intensity, I, is removed since it is a constant value at each pixel for all three colour channels, and the same is true for the shading. While the assumptions above are restrictive, they are simply for guiding a model and have been found to not be necessarily strictly true in practice – sensors can be broadband and light can be any illuminant with chromaticity fairly close to the Planckian locus.

2.2 Entropy Minimization

Simplifying eq.(3) by taking logs, we arrive at a model for pixel log-RGB as follows:

$$\rho_k = \log(c_k) = \log(s_k/s_p) + (e_k - e_p)/T \qquad (4)$$

where $s_k = k_1 \lambda^{-5} S(\lambda_k) q_k$, $s_M = \sqrt[3]{\prod_{j=1}^{3} s_j}$, $e_k = -k_2/\lambda_k$, and $e_k = -k_2/3\sum_{j=1}^{p} \lambda_j$. It can be easily seen that eq.(4) is a straight line parametrized by T. The direction of this line is defined by the direction of vector $(e_k - e_p)$ which is independent of surface. Therefore illumination invariance (intrinsic image) can be achieved by projecting ρ_k to the direction $(e-e_p)^{\perp}$ orthogonal to $(e-e_p)$, which cancels the affect of changes in T.

Direction $(e-e_p)^{\perp}$ can be found by *calibrating* the camera (i.e. dermoscope, here). We, however, follow [8] and use entropy as internal evidence in the image itself to find the invariant direction and optimal projection, in each single image. We project ρ_k, the 2-D log chromaticity representation of the image, over all possible directions from 0° to 180° and choose the direction which has minimum entropy as the optimal one for projection. The result of projection onto the 1-D direction is a 1-D intrinsic image, χ, invariant to all illumination effects such as shading, shadows, specular highlights, etc. The interested reader is advised to refer to [8] for further details of this procedure.

2.3 Geometric–mean

According to [8], the quality of the 1-D invariant image is dependent on the colour channel that is chosen as the divisor. To not rely on any particular colour channel, we divide not by R_p but by the geometric mean $\mu(x,y) = (\prod_{k=3}^{3} R_k)^{\frac{1}{3}}$ at each pixel, for which the invariance properties above persist: $\psi_k(x,y) \equiv \log[R_k(x,y)/\mu(x,y)]$. Then ψ is a 3-vector; it is orthogonal to $(1,1,1)$. Therefore instead of 3-vectors one can easily treat these as 2-vector values, lying in the plane orthogonal to $(1,1,1)$: if the 3×3 projector onto that 2-D subspace is P, then the singular value decomposition of $P = UU^T$, where U is a 3×2 matrix. We project onto 2-D vectors ϕ in the plane coordinate system via U^T:

$$\psi_k(x,y) = \log[R_k(x,y)/\mu(x,y)]; \quad \phi = U^T \psi \qquad (5)$$

2.4 Illumination Normalization

Our method for attenuation of lighting effects is inspired by the work of [10, 7]. Both methods proposed to normalize the uneven illumination in monochromatic images by first, estimating the local illumination and then, normalizing it over the original

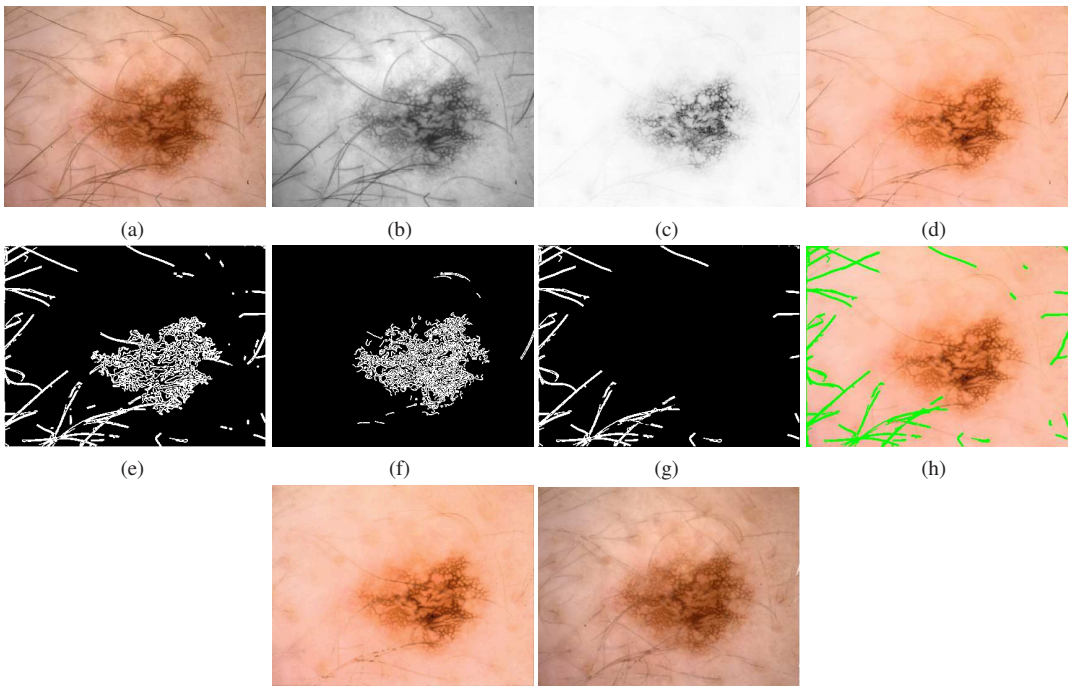

Figure 2. *(a) input image; (b) Value channel of HSV space; (c) χ the intrinsic image - (d) attenuation of shading by using our approach; (e) edge map of V channel (HSV) after shading attenuation; (f) edge map of intrinsic image; (g-h) the difference of edge maps corresponds to the remaining hairs on the image; (i) inpainting the hair masked by g; (j) output of Dullrazor [6] on original image (compare this with (i), outcome of our approach)*

image. Soille [10] used a morphological closing operation to estimate the local illumination, while Cavalcanti et al. [7] tried to model the illumination by a quadratic function of spatial location.

Both methods produce unsatisfactory results for skin images containing lesions, and in particular in the presence of artifacts such as hairs. We, on the other hand, propose to normalize the illumination based on the distribution of intensity values in intrinsic image. In keeping with [10, 7], we convert the image from original RGB to the HSV colour space. The V channel, represents luminance information and it is independent of chrominance information. As noted by Soille [10], the V channel provides high visibility of shading effects. Moreover, as noted by Skarbek and Koschan [11], "the hue channel (for matte surface while ignoring ambient light) is invariant to changes of surface orientation relatively to the light source", discounting shading and shadows.

Figs. 2(b, c) are respectively the Value channel, and χ intrinsic image. We first normalize the intensity values in both monochromatic images, V and χ. Next, the histogram of V is mapped to the histogram of the intrinsic image χ. Finally, the original V channel is replaced with this new (normalized) V channel and the image from HSV is converted to RGB colour space. As can be seen from Fig. 2(d), the effect of shading and intensity falloff is significantly attenuated.

An interesting observation can be made: In the image generated via our proposed method, not only is it shading free but also is free of thin and short hairs, to a degree which is comparable to the achievement of dedicated hair removal algorithms. Note that by examination, we see that the intrinsic image is almost completely free of hairs – see Fig. 2(c). We plan to further study this important and interesting side effect of our method.

We take advantage of this observation to create an artifact free image. Extracting the edge map of our normalized V (i.e. V channel of shading free image, shown in Fig. 2(e)), and comparing to the edge map of the intrinsic image Fig. 2(f), one can easily recognise that the difference between the two corresponds to hairs. Fig. 2(g) is the "hair mask" created by subtracting two edge maps (we dilated the edges before subtraction and applied morphological opening after subtraction to remove small objects). Fig. 2(h) highlights the hair mask in green on the shading-attenuated skin lesion image.

With the hair mask, one can use e.g. inpainting method [12] and *paint* over the hair pixels. Fig. 2(i) is created by using an implementation[1] of inpainting approach – compare the results with Fig. 2(j) obtained by applying the celebrated and highly recognized hair removal software[2], Dullrazor [6]. Note that, in our experiments, it was good enough to set hair pixel colours to zero. Because, we are using Otsu's [13] grey-level thresholding method for segmentation which assumes the lesion is darker than its surrounding, and for this reason zero valued pixels (i.e. detected hairs) will be detected as background.

A final note on this section: our method should not be considered as a hair removal algorithm. It can however facilitate the process. Our proposed approach to deal with images with hair is to first apply any hair removal method, such as [5], and then follow with our lighting artifact attenuation. At this stage, one could take our edge map subtraction approach as a post-process, to remove the remaining hairs in the image.

[1] http://www.cc.gatech.edu/∼sooraj/inpainting/
[2] http://www.dermweb.com/dull_razor/

3. A Novel Colour to Grey–scale Conversion

In the process of automatic analysis of dermoscopic skin images, often a monochromatic image of skin lesion is required e.g. for segmentation or feature extraction. In particular, most texture extraction methods use only intensity information. It is therefore crucial that the algorithm which converts a colour image to greyscale enhances different structures embedded in the image. Similarly for segmentation, a desired colour representation is one that intensifies the contrast between the lesion and the normal skin, whether the segmentation method uses a monochromatic image or any trichromatic colorspace, or even a multi-spectral representation.

We propose a new greyscale conversion method that is based on the optics of human skin and it has direct biological underpinnings. Using this greyscale image for skin lesion segmentation and based on simple grey-level thresholding, we achieved results outperforming the state of the art.

This greyscale conversion provides higher separability between lesion and normal skin. We hypothesize that it would improve the performance of any texture extraction method as well, since it suppresses the normal skin while preserves (and in many cases enhances) the structure of lesions (see e.g. Fig. 3(a)).

The basic idea behind our method is inspired by the work of Tsumura et al. [14, 15] which has shown that in a particular novel colour space, pixel triples of human skin live on a plane, with (non-orthogonal) basis vectors assumed attributable to melanin and hemoglobin only.

We here make an observation that the skin plane is narrow along the direction of its second eigenvector and considerably wider along the direction of first eigenvector. In particular for skin lesions, the entire skin colour plane is approximately spanned by its first eigenvector. Therefore, we project the image, after finding the skin plane, to the basis corresponding to the first eigenvector of the data distribution. This process is described next.

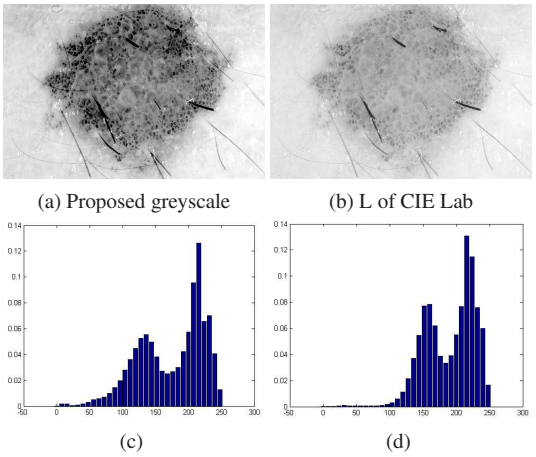

Figure 3. *(c, d) Histogram of (a, b) respectively.*

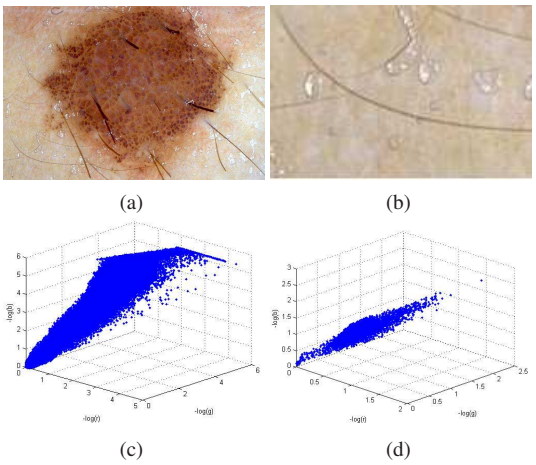

Figure 4. *(a) Image of skin lesion; (b) the bottom right corner of (a) contains healthy skin only; (c, d) Optical density space of (a, b) respectively.*

3.1 Skin Colour Model

Tsumura et al. first suggested using a simple Lambert-Beer type of law for radiance from a multilayer skin surface, resulting from illumination by polarized light [14]. That is, employing a model similar to a simple logarithm model based on optical densities for accounting for light passing for example through multilayer slide film. The transmittance through each colour layer is proportional to the exponential of the negative optical density for that layer.

We utilize the model developed by Hiraoka et al. [16], which formulates a generalization of the fundamental Lambert-Beer law. In this model the spectral reflection of skin (under polarized light) at pixel indexed by (x,y) is given by

$$\begin{aligned} S(x,y,\lambda) \;=\; & \exp\{-\rho_m(x,y)\alpha_m(\lambda)l_m(\lambda) \\ & -\rho_h(x,y)\alpha_h(\lambda)l_h(\lambda)\} \end{aligned} \tag{6}$$

where $\rho_{m,h}$ are densities of melanin and hemoglobin respectively (cm^{-3}), and are assumed to be independent of each other. The cross sectional areas for scattering absorption of melanin and hemoglobin are denoted $\alpha_{m,h}$ (cm^2) and $l_{m,h}$ are the mean pathlength for photons in epidermis and dermis layers, which are used as the depth of the medium in this modified Lambert-Beer law. These quantities are used as well in [15].

By substituting Eq.6 into Eq.3, and taking logs, we arrive at a model for skin pixel log-RGB:

$$\begin{aligned} \log R_k(x,y) = & -\rho_m(x,y)\sigma_m(\lambda_k) - \rho_h(x,y)\sigma_h(\lambda_k) \\ & +\log(k_1 I(x,y)\omega(x,y)) + \left[\log(1/\lambda_k^5) - k_2/(\lambda_k T)\right] \end{aligned} \tag{7}$$

where we have lumped terms $\sigma_m(\lambda_k) = \alpha_m(\lambda_k)l_m(\lambda_k)$, $\sigma_h(\lambda_k) = \alpha_h(\lambda_k)l_h(\lambda_k)$. For notational convenience, denote $u_k = \log(1/\lambda_k^5)$, $e_k = -k_2/\lambda_k$, $m_k = \sigma_m(\lambda_k), h_k = \sigma_h(\lambda_k)$. From eq. 7 it is clear that skin pixels lay on a plane in optical density space: $[-\log R_1, -\log R_2, -\log R_3]$.

Now let us move forward from [15] by making the novel observation mentioned above. Consider Fig. 4(a) as an example; we first extracted the left lower corner of the image which contains only healthy skin (Fig. 4(b)), and plotted its pixel value distribution in optical density space. It can be seen from the plot, Fig. 4(d), that the skin colour plane is wide in one direction and narrow in the other. We can ascertain the importance of one direction against the other by carrying out Principal Component Analysis (PCA) on $\log R_k$: we find that the first-eigenvector component dominates. For the illustrated example, the eigenvalues were $[0.0608, 0.0046, 0.0005]$ (the Total Variance Explained by first component: 0.923). An even more extreme case occurs with the image containing the lesion: Fig. 4(c) illustrates the optical density space and distribution of image data as a whole. While it

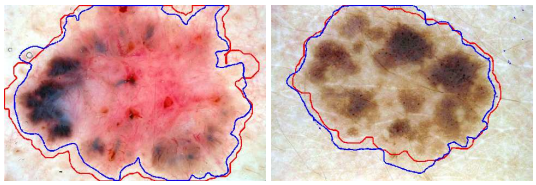

(a) (b)

Figure 5. *Examples of our segmentation results. Blue border: expert segmentation, Red border: our segmentation.*

may not be visually obvious, by carrying PCA, eigenvalues indicate that the data is distributed mostly along a vector (rather than a plane): the eigenvalues are $[2.8878, 0.0434, 0.0057]$ (the Total Variance Explained by first component: 0.983).

The same observation persists in almost all cases we have studied. We conclude, therefore, that the first-eigenvector component explains most of the image and in particular contains most of the information for the lesion. Therefore, by keeping the first principal component (PC), we obtain a greyscale image that expresses the lesion and suppresses the healthy skin surrounding it. This effect can be seen in Fig. 3(a) when compared with Fig. 3(b), the L component of Lab colour space that is usually used as greyscale by many researchers. Moreover, our proposed greyscale provides higher separability between lesion and normal skin. This effect is illustrated in Fig. 3(c) and (d), where the histogram of our proposed greyscale is compared to histogram of L (of CIE Lab). The area of the concavity between the two modes of the histogram is larger for our proposed greyscale. This has a positive contribution to segmentation algorithms based on grey-level thresholding, such as Otsu's [13], as explained in [4]. It is also worth mentioning that the third PC contains mostly the image noise [17] and removing it may have a positive effect (such as de-noising) for the other processes further down the processing pipeline.

In brief, we propose: a greyscale image can be created by carrying out principal component analysis on $\log R_k$ and using the first-eigenvector component.

4. Experiments and Results

For automatic segmentation of lesions, we found that using the greyscale image derived according to § 3.1, and in particular together with our method to attenuate confounding lighting factors, would produce results as good as or better than the state of the art [18, 19] for these dermoscopic images, in a much simpler algorithm (see figure 5 for a few examples).

Here we simply apply Otsu's method [13] for selecting a grey-level threshold. Note that Otsu's method (and also most commercially available automated systems) fails in segmenting low contrast lesions [20]. However our approach achieved very high Precision and Recall, since we discovered that our proposed greyscale supresses the skin around the lesion.

We tested our method on a dataset of images taken from [21, 22] and used by Wighton et al. [18]. They presented a modified random walker (MRW) segmentation where seed points were set automatically based on a lesion probability map (LPM). The LPM was created through a supervised learning algorithm using colour and texture properties.

Table 1 shows results for our method compared to results in [18]. While our method uses a much simpler algorithm and does not require learning, it achieves comparable results. It is worth mentioning, [18] also applied Otsu's method on their lesion probability maps. Their result included in Table 1 under 'Otsu on LPM', with results not nearly as good as ours.

Img.Set	Method	Precision	Recall	F-score
simple	MRW on LPM	0.96	0.95	0.95
	Otsu on LPM	**0.99**	0.86	0.91
	Our Method	0.94	**0.98**	**0.96**
challenging	MRW on LPM	0.83	**0.90**	0.85
	Otsu on LPM	**0.88**	0.68	0.71
	Our Method	0.86	0.89	**0.85**
whole	MRW on LPM	0.87	0.92	0.88
	Otsu on LPM	**0.91**	0.74	0.78
	Our Method	0.88	**0.92**	**0.89**

Table 1: Comparing our segmentation method to the modified random walker (MRW) algorithm and Otsu's thresholding, on lesion probability map (LPM) [18]. The dataset consists of 100 challenging and 20 easy to segment images. An image is considered challenging if any of the following conditions is true: "1) the contrast between the skin and lesion is low, 2) there is significant occlusion by either oil or hair, 3) the entire lesion is not visible, 4) the lesion contains variegated colours or 5) the lesion border is not clearly defined" [18]. Note that our method consistently produces higher F-measures notwithstanding its simplicity and speed.

Method	Sensitivity	Specificity
Our Method	**0.92**	0.88
Multi–layer tree [19]	0.89	0.90
G-Log/LDA [23]	0.88	0.88
KPP [24]	0.71	0.79
DTEA [25]	0.64	**0.99**
SRM [26]	0.77	0.95
JSEG [27]	0.678	**0.99**
FSN [28]	0.81	0.93

Table 2: Comparing our segmentation method to the Multi-level feature extraction method [19], and the output of six other methods, reported together in [19]. Note that our method has highest sensitivity whereas its specificity is comparable to other methods.

We also compare our results with those in [19]. "They proposed a novel tree structure based representation of the lesion growth pattern by matching every pixel sub-cluster with a node in the tree structure" [19]. This multilayer tree is employed to extract sets of features, which are used then, in a supervised learning framework, to segment lesions. They compared sensitivity and specificity of their segmentation results with six other skin lesion segmentation methods. See table 2 and references therein.

5. Conclusions

Automatic analysis of dermoscopy images is subject to error due to its difficulty and the subjectivity of visual interpretation. The development of reliable, effective and feature-preserving pre–processing methods can improve the overall performance.

We have proposed a new pre–processing scheme; a double component process which succeeds in: i) Normalizing intensity falloff, as well as attenuating shading and other confounding factors from dermoscopy images. ii) Colour-to-greyscale conversion which is aimed at intensifying the separation between lesion and healthy skin surrounding it. The new greyscale also amplifies the

underlying structure of lesion.

In the lesion segmentation task, our pre–processing scheme is shown to improve accuracy of segmentation.

Future work will include examination of the effect of our proposed greyscale for feature extraction. We would also like to investigate the effect and possible application of deriving intrinsic images using entropy minimization aimed at removing artifacts such as hair in an image.

References

[1] A. Jemal, R. Siegel, J. Xu, and E. Ward. Cancer statistics, 2010. *CA: A Cancer J. for Clinicians*, 60(5):277–300, 2010.

[2] I. Maglogiannis and C.N. Doukas. Overview of advanced computer vision systems for skin lesions characterization. *IEEE Trans. Inf. Technol. Biomed.*, 13(5):721–733, 2009.

[3] H. Iyatomi, M.E. Celebi, G. Schaefer, and M. Tanaka. Automated color calibration method for dermoscopy images. *The J. of the Compu. Med. Imag. Soc.*, 35(2):89–98, 2011.

[4] D.D. Gmez, C. Butakoff, B.K. Ersbll, and W. Stoecker. Independent histogram pursuit for segmentation of skin lesions. *IEEE Trans. Bio-Med. Eng.*, 55(1):157–161, 2008.

[5] H. Zhou, M. Chen, J.M. Gass, R.and Rehg, L. Ferris, J. Ho, and L. Drogowski. Feature-preserving artifact removal from dermoscopy images. volume 6914, pages 69141B–69141B–9. SPIE, 2008.

[6] T. Lee, V. Ng, R. Gallagher, and D. Coldman, A.and McLean. Dullrazor: A software approach to hair removal from images. *Computers in Biology and Medicine*, 27(6):533–543, 1997.

[7] Pablo G. Cavalcanti, Jacob Scharcanski, and Carlos B. O. Lopes. Shading attenuation in human skin color images. In *Proc. of the 6th Intl. Conf. Advances in visual computing - Volume Part I*, pages 190–198. Springer-Verlag, 2010.

[8] G.D. Finlayson, M.S. Drew, and C. Lu. Intrinsic images by entropy minimization. In *ECCV 2004: European Conf. on Computer Vision*, pages 582–595, 2004.

[9] G.D. Finlayson, M.S. Drew, and B.V. Funt. Spectral sharpening: sensor transformations for improved color constancy. *J. Opt. Soc. Am. A*, 11(5):1553–1563, 1994.

[10] P. Soille. Morphological operation. In B. Jahne, H. Haubecker, and P. Geibler, editors, *Handbook of Computer Vision and Applications*, volume 2, pages 627–682. Academic Press San Diego, 1999.

[11] Wladyslaw Skarbek and Andreas Koschan. Colour image segmentation - a survey. Technical, Institute of Technical Informatics, University of Berlin, 1994.

[12] A. Criminisi, P. Perez, and K. Toyama. Object removal by exemplar-based inpainting. In *Comput. Vision and Pattern Recog., 2003. Proc. IEEE Compu. Soc. Conf.*, volume 2, pages II–721, 2003.

[13] N. Otsu. A threshold selection method from gray-level histograms. *IEEE Trans. on Systems, Man and Cybernetics*, 9(1):62–66, 1979.

[14] N. Tsumura, H. Haneishi, and Y. Miyake. Independent-component analysis of skin color image. *J. of the Optical Soc. of Amer. A*, 16:2169–2176, 1999.

[15] N. Tsumura, N. Ojima, K. Sato, M. Shiraishi, H. Shimizu, H. Nabeshima, S. Akazaki, K. Hori, and Y. Miyake. Image-based skin color and texture analysis/synthesis by extracting hemoglobin and melanin information in the skin. *ACM Trans. Graph.*, 22:770–779, 2003.

[16] M. Hiraoka, M. Firbank, M. Essenpreis, M. Cope, S.R. Arrige, P.V.D. Zee, and D.T. Delpy. A Monte Carlo investigation of optical pathlength in inhomogeneous tissue and its application to near-infrared spectroscopy. *Phys. Med. Biol.*, 38:1859–1876, 1993.

[17] P. Schmid. Segmentation of digitized dermatoscopic images by two-dimensional color clustering. *Med. Imag., IEEE Trans.*, 18(2):164–171, 1999.

[18] P. Wighton, M. Sadeghi, T.K. Lee, and M.S. Atkins. A fully automatic random walker segmentation for skin lesions in a supervised setting. In *MICCAI*, pages 1108–1115, 2009.

[19] S. Khakabi, P. Wighton, T.K. Lee, and Atkins M.S. Multilevel feature extraction for skin lesion segmentation in dermoscopic images. In *Proc. SPIE 8315, 83150E*, 2012.

[20] A. Perrinaud, O. Gaide, L. French, J. Saurat, A. Marghoob, and R. Braun. Can automated dermoscopy image analysis instruments provide added benefit for the dermatologist? *B. J. of Dermatology*, 157(5):926–933, 2007.

[21] G. Argenziano, H.P. Soyer, and et al. *"Interactive Atlas of Dermoscopy (Book and CD-ROM)"*. Edra Med. Pub., 2000.

[22] H.P. Soyer, G. Argenziano, and et. al. *"Dermoscopy of Pigmented Skin Lesions."*. Edra Med. Pub., 2000.

[23] P. Wighton, T.K. Lee, H. Lui, D.I. McLean, and M.S. Atkins. Generalizing common tasks in automated skin lesion diagnosis. *IEEE Trans. Inf. Technol. Biomed.*, 15(4):622 –629, 2011.

[24] H. Zhou, M. Chen, L. Zou, R. Gass, L. Ferris, L. Drogowski, and J.M. Rehg. Spatially constrained segmentation of dermoscopy images. In *5th IEEE Intl. SYM. on BioMed. Imag.: From Nano to Macro, 2008. ISBI*, pages 800 –803, 2008.

[25] M.E. Celebi, Y.A. Aslandogan, and P.R. Bergstresser. Unsupervised border detection of skin lesion images. In *Intl. Conf. Inf. Technol.: Coding and Computing, 2005. ITCC*, volume 2, pages 123 – 128 Vol. 2, 2005.

[26] Hitoshi Iyatomi, Hiroshi Oka, M Emre Celebi, Masahiro Hashimoto, Masafumi Hagiwara, Masaru Tanaka, and Koichi Ogawa. An improved internet-based melanoma screening system with dermatologist-like tumor area extraction algorithm. *The J. of the Compu. Med. Imag. Soc.*, 32(7):566–579, 2008.

[27] M.E. Celebi, H.A. Kingravi, H. Iyatomi, Y.A. Aslandogan, W.V. Stoecker, R.H. Moss, J.M. Malters, J.M. Grichnik, A.A. Marghoob, H.S. Rabinovitz, and S.W. Menzies. Border detection in dermoscopy images using statistical region merging. *Skin research and technol.: J. of Intl. Soc. for Bioeng. and the Skin (ISBS)*, 14(3):347–353, 2008.

[28] M.E. Celebi, S. Hwang, H. Iyatomi, and G. Schaefer. Robust border detection in dermoscopy images using threshold fusion. In *2010 17th IEEE Intl. Conf. Image Process. (ICIP)*, pages 2541 –2544, 2010.